STRUCTURAL DETERMINATION AND ANALYSIS OF SOME NEW SCHIFF BASE AND TRIANGULO-TRIRUTHENIUM COMPOUNDS

YEAP CHIN SING

UNIVERSITI SAINS MALAYSIA
2011

STRUCTURAL DETERMINATION AND ANALYSIS OF SOME NEW SCHIFF BASE AND TRIANGULO-TRIRUTHENIUM COMPOUNDS

by

YEAP CHIN SING

Thesis submitted in fulfilment of the requirements
for the degree of
Master of Science

January 2011

ACKNOWLEDGEMENTS

Specially, I would like to thank my supervisor, Professor Fun Hoong Kun and co-supervisor, Professor Omar bin Shawkataly for their understanding, indispensable guidance and unconditional commitment. Appreciation is extended to Dr. Madhukar Hemamalini and Dr. Reza Kia, Postdoctoral Research Fellows at X-ray Crystallography Unit, School of Physics, Universiti Sains Malaysia (USM) and also his friend Dr. Hadi Kargar from Iran for their useful guidance and the synthesis works of Schiff base samples for the success of this research. Additional thanks to Dr. Imthyaz Ahmed Khan and Dr. Mohd. Aslam A. Pankhi Postdoctoral Research Fellows from School of Distance Education for useful guidance, encouragement and the synthesis works of *triangulo*-triruthenium samples in this research.

For the financial support of this successful research, I would like to express my grateful to the Malaysian Government and USM for the post of research officer through Science Fund grant No. 305/PFIZIK/613312 and also the USM Fellowship. Special acknowledgement is due to Institute of Graduate Studies (IPS) and School of Physics, USM for giving me the opportunity to complete my Masters study.

My sincere thanks to my fellow friends and lab assistants at the X-ray crystallography lab for their useful advices and co-operation throughout my studies in X-ray crystallography lab.

Finally, I would like to thank my parents and all my friends for their understanding, encouragement and moral support which provided me with endless sources of inspiration throughout my studies.

TABLE OF CONTENTS

		Page
Acknowledgements		ii
Table of Contents		iii
List of Tables		x
List of Figures		xiii
List of Plates		xxi
Abstrak		xxii
Abstract		xxiv
CHAPTER 1 – INTRODUCTION		1
1.1	X-rays	2
1.2	Crystal Structure	4
1.3	Reciprocal Lattice	5
1.4	X-ray Diffraction	6
1.5	Superposition of waves	8
1.6	Scattering Factor	10
1.7	Structure Factor	11
1.8	Friedel's Law	13
1.9	Electron Density	15
1.10	Patterson Method (Heavy Atom)	17
1.11	Direct Methods	19
1.12	Data Reduction	21
1.13	Refinement	24
1.14	Disorder	26

1.15 Twinning 27

1.16 Ring Conformations 31

1.17 Schiff Base 35

1.18 *Triangulo*-Triruthenium 36

1.19 Research Objective 37

CHAPTER 2 – MATERIALS AND METHODS 38

2.1 Hardware Overview: SMART APEX II System 39

2.1.1 APEX II CCD Detector 41

2.1.2 3-Axis SMART Goniometer 41

2.1.3 X-ray Source 41

2.1.4 K780 X-ray Generator 42

2.1.5 Timing Shutter and Collimator 42

2.1.6 Video Camera 43

2.1.7 D8 Controller 43

2.1.8 Radiation Safety Enclose with Interlock and Warning Lights 43

2.1.9 Refrigerated Recirculator for the Detector 44

2.1.10 Computer 44

2.1.11 Accessories (Low-Temperature Device) 44

2.2 Software Overview 45

2.2.1 The Server Computer 45

2.2.2 The Client Computer 46

2.3 Methodology 48

2.4 Software 50

2.4.1 Space Group Determination 50

2.4.2 Trial Structure Solution 51

2.4.3 Structure Refinement 51

2.4.4 Accessing the Solution 52

2.4.5 Preparation of Tables and Plots 53

2.4.6 Command 54

2.5 Preparation and Crystallization of Compounds 55

2.5.1 4,4',5,5'-Tetramethyl-2,2'-[1,1'-(propane-1,3-diyldinitrilo) diethylidyne]diphenol; (I) 55

2.5.2 5,5'-Dimethoxy-2,2'-[2,2-dimethylpropane-1,3-diylbis (nitrilomethylidyne)]diphenol; (II) 55

2.5.3 4,4'-Dichloro-2,2'-[2,2-dimethylpropane-1,3-diylbis(nitrilomethylidyne)]diphenol; (III) 56

2.5.4 6,6'-Dimethoxy-2,2'-[2,2-dimethylpropane-1,3-diylbis(nitrilomethylidyne)]diphenol; (IV) 56

2.5.5 {6,6'-Dimethoxy-2,2'-[2,2-dimethylpropane-1,3-diylbis(nitrilomethylidyne)]diphenolato}nickel(II) 1.78-hydrate; (V) 56

2.5.6 2-(1*H*-Benzoimidazol-2-yl)-6-ethoxy-phenol; (VI) 57

2.5.7 4-[(2,4-Dihydroxybenzylidene)-ammonio]benzene sulfonate trihydrate; (VII) 57

2.5.8 *N*,*N*'-Bis(2,6-dichlorobenzylidene)1,2-diaminopropane; (VIII) 57

2.5.9 Undecacarbonyl-1κ^3C,2κ^4C,3κ^4C-[tris(3-chlorophenyl) phosphine-1κP]-*triangulo*-triruthenium(0); (IX) 58

2.5.10 Decacarbonyl-1κ^3C,2κ^3C,3κ^4C-bis[tris(3-chlorophenyl) phosphine]-1κP,2κP-*triangulo*-triruthenium(0) monohydrate; (X) 58

2.5.11 Undecacarbonyl-1κ^3C,2κ^4C,3κ^4C-[tris(4-methylphenyl) arsine-1κAs]-*triangulo*-triruthenium(0); (XI) 59

2.5.12 [μ-Bis(diphenylphosphino)methane-1:2κ^2P:P']-nonacarbonyl-1κ^3C,2κ^3C,3κ^3C-[tris(4-methylphenyl) arsine-3κAs]-*triangulo*-triruthenium(0); (XII) 59

2.5.13 Bis[μ-bis(diphenylphosphino)methane-1:2κ^2P:P']-nonacarbonyl-1κ^3C,2κ^3C,3κ^3C-[tris(4-methoxyphenyl) arsine-3κAs]-*triangulo*-triruthenium(0) dichloromethane solvate; (XIII) 60

2.5.14 Bis[μ-Bis(diphenylarsino)methane-1:2κ^2As:As']-nonacarbonyl-1κ^3C,2κ^3C,3κ^3C-[tris(4-methoxyphenyl) arsine-3κAs]-*triangulo*-triruthenium(0) dichloromethane solvate; (XIV) 60

2.5.15 [μ-Bis(diphenylarsino)methane-1:2κ^2As:As']-nonacarbonyl-1κ^3C,2κ^3C,3κ^3C-[bis(4-methoxyphenyl) phenylphosphine-3κP]-*triangulo*-triruthenium(0) dichloromethane 0.15-solvate; (XV) 61

2.5.16 [μ-Bis(diphenylarsino)methane-1:2κ^2As:As']-nonacarbonyl-1κ^3C,2κ^3C,3κ^3C-[tris(4-methylphenyl) phosphine-3κP]-*triangulo*-triruthenium(0); (XVI) 61

2.5.17 [μ-Bis(diphenylarsino)methane-1:2κ^2As:As']-nonacarbonyl-1κ^3C,2κ^3C,3κ^3C-[tris(4-flurophenyl) phosphine-3κP]-*triangulo*-triruthenium(0); (XVII) 62

2.5.18 [μ-Bis(diphenylarsino)methane-1:2κ^2As:As']-nonacarbonyl-1κ^3C,2κ^3C,3κ^3C-[(pentafluorophenyl) diphenylphosphine-3κP]-*triangulo*-triruthenium(0) chloroform monosolvate; (XVIII) 62

2.5.19 [μ-Bis(diphenylarsino)methane-1:2κ^2As:As']-nonacarbonyl-1κ^3C,2κ^3C,3κ^3C-[(2-methoxyphenyl) diphenylphosphine-3κP]-*triangulo*-triruthenium(0); (XIX) 63

2.5.20 Bis[μ-bis(diphenylarsino)methane-1:2κ^2As:As']-nonacarbonyl-1κ^3C,2κ^3C,3κ^3C-[tris(4-chlorophenyl) phosphine-3κP]-*triangulo*-triruthenium(0) chloroform monosolvate; (XX) 63

2.5.21 [Benzyldiphenylphosphine-3κP][μ-Bis(diphenylarsino) methane-1:2κ^2As:As']-nonacarbonyl-1κ^3C,2κ^3C,3κ^3C-*triangulo*-triruthenium(0); (XXI) 64

2.5.22 [μ-Bis(diphenylarsino)methane-1:2κ^2*As*:*As*'][(4-bromophenyl)diphenylphosphine-3κ*P*]-nonacarbonyl-1κ^3*C*,2κ^3*C*,3κ^3*C*-*triangulo*-triruthenium(0) chloroform 0.30-solvate; (XXII) 64

2.5.23 [μ-Bis(diphenylarsino)methane-1:2κ^2*As*:*As*']-nonacarbonyl-1κ^3*C*,2κ^3*C*,3κ^3*C*-[triphenylphosphite-3κ*P*]-*triangulo*-triruthenium(0); (XXIII) 65

2.5.24 [μ-Bis(diphenylarsino)methane-1:2κ^2*As*:*As*']-nonacarbonyl-1κ^3*C*,2κ^3*C*,3κ^3*C*-[diphenyl(phenyl sulfanylmethyl)phosphine-3κ*P*]-*triangulo*-triruthenium(0) chloroform hemisolvate; (XXIV) 65

2.5.25 [μ-Bis(diphenylarsino)methane-1:2κ^2*As*:*As*']-nonacarbonyl-1κ^3*C*,2κ^3*C*,3κ^3*C*-[tricyclohexyl phosphine-3κ*P*]-*triangulo*-triruthenium(0); (XXV) 66

2.5.26 [μ-Bis(diphenylarsino)methane-1:2κ^2*As*:*As*']-nonacarbonyl-1κ^3*C*,2κ^3*C*,3κ^3*C*-[triphenylstibine-3κ*Sb*]-*triangulo*-triruthenium(0); (XXVI) 66

CHAPTER 3 – RESULTS AND DISCUSSION 67

3.1 4,4',5,5'-Tetramethyl-2,2'-[1,1'-(propane-1,3-diyldinitrilo) diethylidyne]diphenol; (I) 67

3.2 5,5'-Dimethoxy-2,2'-[2,2-dimethylpropane-1,3-diylbis (nitrilomethylidyne)]diphenol; (II) 72

3.3 4,4'-Dichloro-2,2'-[2,2-dimethylpropane-1,3-diylbis(nitrilomethylidyne)]diphenol; (III) 77

3.4 6,6'-Dimethoxy-2,2'-[2,2-dimethylpropane-1,3-diylbis(nitrilomethylidyne)]diphenol; (IV) 82

3.5 {6,6'-Dimethoxy-2,2'-[2,2-dimethylpropane-1,3-diylbis(nitrilomethylidyne)]diphenolato}nickel(II) 1.78-hydrate; (V) 87

3.6 2-(1*H*-Benzoimidazol-2-yl)-6-ethoxy-phenol; (VI) 92

3.7 4-[(2,4-Dihydroxybenzylidene)-ammonio]benzene sulfonate trihydrate; (VII) 97

3.8 *N*,*N*'-Bis(2,6-dichlorobenzylidene)1,2-diaminopropane; (VIII) 101

3.9	Undecacarbonyl-1κ^3C,2κ^4C,3κ^4C-[tris(3-chlorophenyl) phosphine-1κP]-*triangulo*-triruthenium(0); (IX)	104
3.10	Decacarbonyl-1κ^3C,2κ^3C,3κ^4C-bis[tris(3-chlorophenyl) phosphine]-1κP,2κP-*triangulo*-triruthenium(0) monohydrate; (X)	108
3.11	Undecacarbonyl-1κ^3C,2κ^4C,3κ^4C-[tris(4-methylphenyl) arsine-1κAs]-*triangulo*-triruthenium(0); (XI)	114
3.12	[μ-Bis(diphenylphosphino)methane-1:2κ^2P:P']-nonacarbonyl-1κ^3C,2κ^3C,3κ^3C-[tris(4-methylphenyl) arsine-3κAs]-*triangulo*-triruthenium(0); (XII)	118
3.13	Bis[μ-bis(diphenylphosphino)methane-1:2κ^2P:P']-nonacarbonyl-1κ^3C,2κ^3C,3κ^3C-[tris(4-methoxyphenyl) arsine-3κAs]-*triangulo*-triruthenium(0) dichloromethane solvate; (XIII)	123
3.14	Bis[μ-Bis(diphenylarsino)methane-1:2κ^2As:As']-nonacarbonyl-1κ^3C,2κ^3C,3κ^3C-[tris(4-methoxyphenyl) arsine-3κAs]-*triangulo*-triruthenium(0) dichloromethane solvate; (XIV)	128
3.15	[μ-Bis(diphenylarsino)methane-1:2κ^2As:As']-nonacarbonyl-1κ^3C,2κ^3C,3κ^3C-[bis(4-methoxyphenyl) phenylphosphine-3κP]-*triangulo*-triruthenium(0) dichloromethane 0.15-solvate; (XV)	133
3.16	[μ-Bis(diphenylarsino)methane-1:2κ^2As:As']-nonacarbonyl-1κ^3C,2κ^3C,3κ^3C-[tris(4-methylphenyl) phosphine-3κP]-*triangulo*-triruthenium(0); (XVI)	137
3.17	[μ-Bis(diphenylarsino)methane-1:2κ^2As:As']-nonacarbonyl-1κ^3C,2κ^3C,3κ^3C-[tris(4-flurophenyl) phosphine-3κP]-*triangulo*-triruthenium(0); (XVII)	141
3.18	[μ-Bis(diphenylarsino)methane-1:2κ^2As:As']-nonacarbonyl-1κ^3C,2κ^3C,3κ^3C-[(pentafluorophenyl) diphenylphosphine-3κP]-*triangulo*-triruthenium(0) chloroform monosolvate; (XVIII)	145
3.19	[μ-Bis(diphenylarsino)methane-1:2κ^2As:As']-nonacarbonyl-1κ^3C,2κ^3C,3κ^3C-[(2-methoxyphenyl) diphenylphosphine-3κP]-*triangulo*-triruthenium(0); (XIX)	150
3.20	Bis[μ-bis(diphenylarsino)methane-1:2κ^2As:As']-nonacarbonyl-1κ^3C,2κ^3C,3κ^3C-[tris(4-chlorophenyl) phosphine-3κP]-*triangulo*-triruthenium(0) chloroform monosolvate; (XX)	154

3.21 [Benzyldiphenylphosphine-3κP][μ-Bis(diphenylarsino) methane-1:2$\kappa^2 As$:As']-nonacarbonyl-1$\kappa^3 C$,2$\kappa^3 C$,3$\kappa^3 C$-*triangulo*-triruthenium(0); (XXI) 160

3.22 [μ-Bis(diphenylarsino)methane-1:2$\kappa^2 As$:As'][(4-bromophenyl)diphenylphosphine-3κP]-nonacarbonyl-1$\kappa^3 C$,2$\kappa^3 C$,3$\kappa^3 C$-*triangulo*-triruthenium(0) chloroform 0.30-solvate; (XXII) 164

3.23 [μ-Bis(diphenylarsino)methane-1:2$\kappa^2 As$:As']-nonacarbonyl-1$\kappa^3 C$,2$\kappa^3 C$,3$\kappa^3 C$-[triphenylphosphite-3κP]-*triangulo*-triruthenium(0); (XXIII) 169

3.24 [μ-Bis(diphenylarsino)methane-1:2$\kappa^2 As$:As']-nonacarbonyl-1$\kappa^3 C$,2$\kappa^3 C$,3$\kappa^3 C$-[diphenyl(phenyl sulfanylmethyl)phosphine-3κP]-*triangulo*-triruthenium(0) chloroform hemisolvate; (XXIV) 174

3.25 [μ-Bis(diphenylarsino)methane-1:2$\kappa^2 As$:As']-nonacarbonyl-1$\kappa^3 C$,2$\kappa^3 C$,3$\kappa^3 C$-[tricyclohexyl phosphine-3κP]-*triangulo*-triruthenium(0); (XXV) 179

3.26 [μ-Bis(diphenylarsino)methane-1:2$\kappa^2 As$:As']-nonacarbonyl-1$\kappa^3 C$,2$\kappa^3 C$,3$\kappa^3 C$-[triphenylstibine-3κSb]-*triangulo*-triruthenium(0); (XXVI) 185

CHAPTER 4 – CONCLUSION 189

4.1 Conclusion 189

4.2 Recommendation for Future Research 191

References 192

List of Publications 198

LIST OF TABLES

		Page
Table 2.1	The commands used in instruction file	54
Table 3.1	Crystal data and structure refinement of compound (I)	67
Table 3.2	Hydrogen-bond geometry (Å,°) of compound (I)	68
Table 3.3	Crystal data and structure refinement of compound (II)	72
Table 3.4	Hydrogen-bond geometry (Å,°) of compound (II)	74
Table 3.5	Crystal data and structure refinement of compound (III)	77
Table 3.6	Hydrogen-bond geometry (Å,°) of compound (III)	79
Table 3.7	Crystal data and structure refinement of compound (IV)	82
Table 3.8	Selected geometric parameters (Å) associated with π···π stacking interactions between the planar sections of C1A−C6A−C7A−N1A and C5B−C6B−C7B−N1B of compound (IV)	84
Table 3.9	Hydrogen-bond geometry (Å,°) of compound (IV)	84
Table 3.10	Crystal data and structure refinement of compound (V)	87
Table 3.11	Hydrogen-bond geometry (Å,°) of compound (V)	89
Table 3.12	Crystal data and structure refinement of compound (VI)	92
Table 3.13	Hydrogen-bond geometry (Å,°) of compound (VI)	94
Table 3.14	Crystal data and structure refinement of compound (VII)	97
Table 3.15	Hydrogen-bond geometry (Å,°) of compound (VII)	99
Table 3.16	Crystal data and structure refinement of compound (VIII)	101

Table 3.17	Crystal data and structure refinement of compound (IX)	104
Table 3.18	Hydrogen-bond geometry (Å,°) of compound (IX)	106
Table 3.19	Crystal data and structure refinement of compound (X)	108
Table 3.20	Hydrogen-bond geometry (Å,°) of compound (X)	110
Table 3.21	Crystal data and structure refinement of compound (XI)	114
Table 3.22	Hydrogen-bond geometry (Å,°) of compound (XI)	116
Table 3.23	Crystal data and structure refinement of compound (XII)	118
Table 3.24	Hydrogen-bond geometry (Å,°) of compound (XII)	120
Table 3.25	Crystal data and structure refinement of compound (XIII)	123
Table 3.26	Hydrogen-bond geometry (Å,°) of compound (XIII)	125
Table 3.27	Crystal data and structure refinement of compound (XIV)	128
Table 3.28	Hydrogen-bond geometry (Å,°) of compound (XIV)	130
Table 3.29	Crystal data and structure refinement of compound (XV)	133
Table 3.30	Crystal data and structure refinement of compound (XVI)	137
Table 3.31	Hydrogen-bond geometry (Å,°) of compound (XVI)	139
Table 3.32	Crystal data and structure refinement of compound (XVII)	141
Table 3.33	Hydrogen-bond geometry (Å,°) of compound (XVII)	143
Table 3.34	Crystal data and structure refinement of compound (XVIII)	145
Table 3.35	Hydrogen-bond geometry (Å,°) of compound (XVIII)	147
Table 3.35	Crystal data and structure refinement of compound (XIX)	150

Table 3.36	Hydrogen-bond geometry (Å,°) of compound (XIX)	152
Table 3.37	Crystal data and structure refinement of compound (XX)	154
Table 3.38	Hydrogen-bond geometry (Å,°) of compound (XX)	156
Table 3.39	Crystal data and structure refinement of compound (XXI)	160
Table 3.40	Hydrogen-bond geometry (Å,°) of compound (XXI)	162
Table 3.41	Crystal data and structure refinement of compound (XXII)	164
Table 3.42	Hydrogen-bond geometry (Å,°) of compound (XXII)	166
Table 3.43	Crystal data and structure refinement of compound (XXIII)	169
Table 3.44	Hydrogen-bond geometry (Å,°) of compound (XXIII)	172
Table 3.45	Crystal data and structure refinement of compound (XXIV)	174
Table 3.46	Hydrogen-bond geometry (Å,°) of compound (XXIV)	176
Table 3.47	Crystal data and structure refinement of compound (XXV)	179
Table 3.48	Hydrogen-bond geometry (Å,°) of compound (XXV)	182
Table 3.49	Crystal data and structure refinement of compound (XXVI)	185
Table 3.50	Hydrogen-bond geometry (Å,°) of compound (XXVI)	187

LIST OF FIGURES

		Page
Fig. 1.1	The process of X-ray crystallography	1
Fig. 1.2	Cross section of filament X-ray tube	3
Fig 1.3	Bragg's law diffraction	6
Fig. 1.4	Ewald sphere, radius $1/\lambda$ and limiting sphere, radius $2/\lambda$	8
Fig. 1.5	Components on the coordinate axes of a sum of vectors are equal to the sums of the components of the individual vectors	9
Fig. 1.6	Atomic scattering factors: (a) stationary atom, $f_{j,\theta}$ (b) atom corrected for thermal vibration, $f_{j,\theta}T_{j,\theta}$	11
Fig. 1.7	Relationship between **F***(hkl)* dan **F** $(\bar{h}\bar{k}\bar{l})$ leading to Friedel's law, from which $\|F(hkl)\|=\|F(\bar{h}\bar{k}\bar{l})\|$	14
Fig. 1.8	Superposition of the *h*0*l*-layers of the reciprocal lattices in a non-merohedral monoclinic (100)-twin	28
Fig. 1.9	Coincidence in every second layer along c* in a partially merohedral twin. The apparent, smaller reciprocal cell is outlined	28
Fig. 1.10	Complete coincidence of the reciprocal lattices of a merohedral (110) twin of a tetragonal crystal with Laue symmetry 4/m. a) hk0-layer of the first component with the twin element shown. b) The corresponding layer in the second component. c) Superposition of the two layers in a 1:1 ratio giving the Laue group 4/mmm	29
Fig. 1.11	Conformations observed for six-member rings. The mirror and twofold symmetries are indicated on the right	32
Fig. 1.12	The three most symmetric conformations observed for five-member rings have the symmetries indicated at the right	33
Fig. 1.13	One octant of the sphere on which the conformations of six-membered rings can be mapped (for a constant Q)	34
Fig. 1.14	The reaction scheme of Schiff base compound	35

Fig. 1.15	The availability of mono-, bis-, and tri- substituted derivatives of $Ru_3(CO)_{12}$	36
Fig. 2.1	*SMART APEX II* scheme	40
Fig. 2.2	*SMART* goniometer components	40
Fig. 2.3	APEX 2 software diagram	47
Fig. 2.4	A basic structure solution flow chart	53
Fig. 3.1	The chemical scheme diagram of compound (I)	67
Fig. 3.2	The molecular structure of (I) with atom labels and 50% probability ellipsoids for non-H atoms. The suffix A corresponds to symmetry code (-*x* + 1, *y*, -*z* + 3/2). Intramolecular interactions are shown as dashed lines	69
Fig. 3.3	The molecular structure of (I) showing the two sides of the molecule are almost perpendicular to each other	69
Fig. 3.4	The crystal packing of (I), viewed down the *b* axis showing chains along the *c* axis and stacking of these chains along the *b* axis. Intramolecular and intermolecular interactions are shown as dashed lines	70
Fig. 3.5	The crystal packing of (I), showing a sheet parallel to the *bc* plane. Intermolecular interactions are shown as dashed lines	71
Fig. 3.6	The chemical scheme diagram of compound (II)	72
Fig. 3.7	The asymmetric unit of compound (II), showing four independent molecules with atom labels. Displacement ellipsoids are drawn at the 40% probability level. Intramolecular interactions are shown as dashed lines	75
Fig. 3.8	Fit of the compound (II) molecule *A* (dashed lines) and *B* (solid lines), showing the difference in conformation between two independent molecules	75
Fig. 3.9	The crystal packing of compound (II), viewed down the *b* axis, showing the $R_2^2(8)$ dimers. Hydrogen bonds are shown as dashed lines	76
Fig. 3.10	The chemical scheme diagram of compound (III)	77

Fig. 3.11	The molecular structure of (III) with atom labels and 50% probability ellipsoids for non-H atoms. Intramolecular interactions are shown as dashed lines	80
Fig. 3.12	Fit of compound (III) molecule *A* (dashed lines) and *B* (solid lines), showing the difference in conformation between two independent molecules	80
Fig. 3.13	The crystal packing of (III), viewed down the *b* axis showing a 3-D network. Intermolecular interactions are shown as dashed lines	81
Fig. 3.14	The chemical scheme diagram of compound (IV)	82
Fig. 3.15	The molecular structure of (IV) with atom labels and 50% probability ellipsoids for non-H atoms. Intramolecular interactions are shown as dashed lines	85
Fig. 3.16	Fit of the title molecule *A* (dashed lines) and *B* (solid lines), showing the difference between two independent molecules	85
Fig. 3.17	The crystal structure of compound (IV), viewed down the *a* axis	86
Fig. 3.18	The chemical scheme diagram of compound (V)	87
Fig. 3.19	The asymmetric unit of compound (V), showing 50% probability displacement ellipsoids and the atomic numbering. Hydrogen bonds are drawn as dashed lines	90
Fig. 3.20	The crystal packing of (V) viewed down the *b* axis, showing one-dimensional extended chains along the *b* axis. Intermolecular interactions are drawn as dashed lines	91
Fig. 3.21	The chemical scheme diagram of compound (VI)	92
Fig. 3.22	The molecular structure of (VI) with atom labels and 50% probability ellipsoids for non-H atoms. Intra- and intermolecular hydrogen bonds are shown as dashed lines. The open bond indicates the minor component of disorder	95
Fig. 3.23	The crystal packing of (VI) viewing down *b* axis showing chains along *b* axis with hydrogen bonds shown as dashed lines. Only major disorder component is shown	96
Fig. 3.24	The chemical scheme diagram of compound (VII)	97

Fig. 3.25	The molecular structure of (VII) with atom labels and 50% probability ellipsoids for non-H atoms. The intramolecular hydrogen bond is shown as a dashed line	99
Fig. 3.26	The crystal packing of (VII), viewed down the *b* axis, showing the molecules linked into a 3-D framework. Intermolecular hydrogen bonds are shown as dashed lines	100
Fig. 3.27	The chemical scheme diagram of compound (VIII)	101
Fig. 3.28	The molecular structure of (VIII) with 50% probability ellipsoids for non-H atoms. All disordered components are shown.	103
Fig. 3.29	The crystal packing of (VIII), viewed down the *a* axis, showing the molecules stacked along the *a* axis. Only the major disordered component is shown	103
Fig. 3.30	The chemical scheme diagram of compound (IX)	104
Fig. 3.31	The molecular structure of (IX) with atom labels and 50% probability ellipsoids for non-H atoms.	106
Fig. 3.32	A pair of molecules is linked into a dimer by intermolecular hydrogen bonds (dashed lines)	107
Fig. 3.33	The chemical scheme diagram of compound (X)	108
Fig. 3.34	The asymmetric unit of compound (X), showing 50% probability displacement ellipsoids and the atomic numbering	111
Fig. 3.35	Fit of compound (IX) (dashed lines) with both sides of the phosphine ligand of compound (X) (solid lines) showing the difference between these two molecules	112
Fig. 3.36	The crystal packing of (X), viewed down the *a* axis, showing the molecules linked into columns along *a* axis. Hydrogen atoms not involved in the hydrogen-bonding (dashed lines) and the solvent molecules have been omitted for clarity	113
Fig. 3.37	The chemical scheme diagram of compound (XI)	114
Fig. 3.38	The molecular structure of (XI) with 30% probability ellipsoids for non-H atoms	116
Fig. 3.39	The crystal packing of (XI), viewed down the *b* axis, showing the molecules stacked down *b* axis	117

Fig. 3.40	The chemical scheme diagram of compound (XII)	118
Fig. 3.41	The molecular structure of (XII) with atom labels and 50% probability ellipsoids for non-H atoms	121
Fig. 3.42	Fit of compound (XI) (dashed lines) with compound (XII) (solid lines), showing the difference between these two molecules	121
Fig. 3.43	The crystal packing of (XII), viewed down the *b* axis, showing the molecular dimers stacked down *b* axis. Hydrogen atoms that not involved in the hydrogen-bonding (dashed lines) have been omitted for clarity	122
Fig. 3.44	The chemical scheme diagram of compound (XIII)	123
Fig. 3.45	The molecular structure of (XIII) with 50% probability ellipsoids for non-H atoms. Atoms with suffix A are generated by the symmetry operation (2 - *x*, 1 - *y*, -*z*)	126
Fig. 3.46	The crystal packing of (XIII), viewed down the *a* axis, showing the molecules linked along *b* axis. Hydrogen atoms that are not involved in the hydrogen-bonding (dashed lines) and solvent molecules have been omitted for clarity	127
Fig. 3.47	The chemical scheme diagram of compound (XIV)	128
Fig. 3.48	The molecular structure of (XIV) with 30% probability ellipsoids for non-H atoms. Atoms with suffix A are generated by the symmetry operation (1 - *x*, 1 - *y*, 1 - *z*)	131
Fig. 3.49	Fit of compound (XIII) (dashed lines) with compound (XIV) (solid lines) showing the similarity of these two molecules	131
Fig. 3.50	The crystal packing of (XIV), viewed down the *a* axis, showing the molecules stacked along *a* axis. The solvent molecules have been omitted for clarity	132
Fig. 3.51	The chemical scheme diagram of compound (XV)	133
Fig. 3.52	The molecular structure of (XV) with 20% probability ellipsoids for non-H atoms	135
Fig. 3.53	The crystal packing of (XV), viewed down the *b* axis, showing the molecules stacked along *b* axis. Hydrogen atoms and the solvent molecules have been omitted for clarity	136

Fig. 3.54	The chemical scheme diagram of compound (XVI)	137
Fig. 3.55	The molecular structure of (XVI) with 20% probability ellipsoids for non-H atoms	140
Fig. 3.56	The crystal packing of (XVI), viewed down the *c* axis, showing the molecules linked along *b*. Hydrogen atoms that are not involved in the hydrogen-bonding (dashed lines) have been omitted for clarity	140
Fig. 3.57	The chemical scheme diagram of compound (XVII)	141
Fig. 3.58	The molecular structure of (XVII) with 20% probability ellipsoids for non-H atoms	143
Fig. 3.59	The crystal packing of (XVII), viewed down the *b* axis, showing the molecules packed into a 3-D framework. Hydrogen atoms not involved in the hydrogen-bonding (dashed lines) have been omitted for clarity	144
Fig. 3.60	The chemical scheme diagram of compound (XVIII)	145
Fig. 3.61	The molecular structure of (XVIII) with 30% probability ellipsoids for non-H atoms. All disorder components are shown	148
Fig. 3.62	The crystal packing of (XVIII), viewed down the *a* axis, showing the molecules linked into a plane parallel to *bc* plane. Hydrogen atoms not involved in the hydrogen-bonding (dashed lines) and the solvent molecules have been omitted for clarity	149
Fig. 3.63	The chemical scheme diagram of compound (XIX)	150
Fig. 3.64	The molecular structure of (XIX) with atom labels and 30% probability ellipsoids for non-H atoms	152
Fig. 3.65	The crystal packing of (XIX), viewed down the *a* axis, showing the molecules linked down *a* axis. Hydrogen atoms that not involved in the hydrogen-bonding (dashed lines) have been omitted for clarity	153
Fig. 3.66	The chemical scheme diagram of compound (XX)	154
Fig. 3.67	The asymmetric unit of compound (XX), showing 50% probability displacement ellipsoids	157
Fig. 3.68	The separate labeling of molecules *A* (top) and *B* (bottom) of compound (XX) for clarity, showing 50% probability displacement ellipsoids	158

Fig. 3.69	The crystal packing of (XX), viewed down the *a* axis, showing the molecules linked into a 3-D framework. Hydrogen atoms that not involved in the hydrogen-bonding (dashed lines) and the solvent molecules have been omitted for clarity	159
Fig. 3.70	The chemical scheme diagram of compound (XXI)	160
Fig. 3.71	The molecular structure of (XXI) with 30% probability ellipsoids for non-H atoms	163
Fig. 3.72	The crystal packing of (XXI), viewed down the *c* axis, showing the molecules linked into a chain. Hydrogen atoms that not involved in the hydrogen-bonding (dashed lines) have been omitted for clarity	163
Fig. 3.73	The chemical scheme diagram of compound (XXII)	164
Fig. 3.74	The molecular structure of (XXII) with atom labels and 20% probability ellipsoids for non-H atoms. All disordered components are shown	167
Fig. 3.75	The crystal packing of (XXII), viewed down the *a* axis, showing the molecules linked into chains along *a* axis. Hydrogen atoms not involved in the hydrogen-bonding (dashed lines) and the solvent molecules have been omitted for clarity	168
Fig. 3.76	The chemical scheme diagram of compound (XXIII)	169
Fig. 3.77	The molecular structure of (XXIII) with 30% probability ellipsoids for non-H atoms. All disordered components are shown	172
Fig. 3.78	The crystal packing of (XXIII), viewed down the *a* axis, showing the molecules stacked along *a* axis. Hydrogen atoms not involved in the hydrogen-bonding (dashed lines) have been omitted for clarity. Only major disordered component is shown	173
Fig. 3.79	The chemical scheme diagram of compound (XXIV)	174
Fig. 3.80	The molecular structure of (XXIV) with 30% probability ellipsoids for non-H atoms. All disordered components are shown	177

Fig. 3.81	The crystal packing of (XXIV), viewed down the *a* axis, showing the molecules linked into a chain along *b* axis by C–H···O contacts (dashed lines); the remaining H atoms and the solvent molecules have been deleted for reasons of clarity. Only major disordered component is shown	178
Fig. 3.82	The chemical scheme diagram of compound (XXV)	179
Fig. 3.83	The molecular structure of (XXV) with 30% probability ellipsoids for non-H atoms. The major (top) and minor (bottom) components are shown	183
Fig. 3.84	The crystal packing of (XXV), viewed down the *c* axis, showing the molecules linked down *a* axis. Hydrogen atoms that not involved in the hydrogen-bonding (dashed lines) have been omitted for clarity. Only the major components are shown	184
Fig. 3.85	The chemical scheme diagram of compound (XXVI)	185
Fig. 3.86	The molecular structure of (XXVI) with 30% probability ellipsoids for non-H atoms	188
Fig. 3.87	The crystal packing of (XXVI), viewed down the *a* axis, showing the molecules linked along the *c* axis. Hydrogen atoms that are not involved in the hydrogen-bonding (dashed lines) have been omitted for clarity	188

LIST OF PLATES

		Page
Plate 2.1	*SMART APEX II* system (USM X-ray Crystallography Lab)	38
Plate 2.2	A reflection photo produced by a good quality crystal	49

PENENTUAN DAN ANALISIS STRUKTUR BARU SEBATIAN SCHIFF BASE DAN *TRIANGULO*-TRIRUTHENIUM

ABSTRAK

Lapan sebatian Schiff base dikaji dalam kajian ini. Mereka terhablur dalam sistem hablur yang biasa iaitu, empat sebatian dalam monoklinik *C*2/*c*, dan masing-masing satu dalam monoklinik *Cc*, $P2_1$ and *Pn* dan triklinik $P\bar{1}$. Salah satu sebatian Schiff base dalam bentuk zwitterion. Struktur bagi dua sebatian Schiff base adalah berantakan. Salah satu sebatian Schiff base adalah hablur kembar rasemik. Unit asimetrik bagi dua sebatian Schiff base mengandungi molekul pelarut air. Semua sebatian Schiff base adalah dalam bentuk konfigurasi *E* mengenai ikatan ganda N=C. Nilai purata bagi jarak ikatan ganda N=C ialah 1.282 Å. Lapan belas sebatian *triangulo*-triruthenium dikaji dalam kajian ini. Kesemuanya terhablur dalam sistem hablur yang biasa iaitu, tujuh sebatian dalam triklinik $P\bar{1}$, tujuh lagi dalam monoklinik $P2_1/c$, dua dalam monoklinik *C*2/*c*, and masing-masing satu dalam ortorombik *Pbca* and $Pca2_1$. Empat struktur sebatian *triangulo*-triruthenium adalah berantakan. Unit asimetrik bagi lapan sebatian mengandungi molekul perlarut seperti air, diklorometana atau kloroform. Semua molekul perlarut berantakan kecuali satu daripada lapan sebatian tersebut adalah tidak berantakan. Salah satu sebatian *triangulo*-triruthenium adalah hablur kembar rasemik dan satu lagi adalah hablur kembar pseudomerohedral. Ligand kumpulan-15 menduduki kedudukan khatulistiwa dalam semua sebatian *triangulo*-triruthenium disebabkan oleh reaksi sterik. Perbezaan yang signifikasi bagi jarak ikatan Ru—Ru dan jarak ikatan dengan sudut ligand karbonil akibat daribada kesan penggantian. Nilai purata jarak ikatan antara tiga Ru—Ru adalah 2.840 Å, 2.860 Å dan 2.878 Å. Jarak ikatan Ru—C axial adalah lebih panjang daripada jarak ikatan Ru—C khatulistiwa. Nilai purata jarak ikatan

Ru—C axial adalah 1.931 Å dan nilai purata jarak ikatan Ru—C khatulistiwa adalah 1.892 Å. Ikatan Ru—C khatulistiwa yang menyambung kepada atom Ru yang menyambung kepada ligand monopenggantian adalah ikatan yang paling pendek bagi kebanyakan sebatian. Nilai purata bagi jarak ikatan Ru—C ini adalah 1.882 Å. Sudut Ru—C—O khatulistiwa adalah hampir linear manakala sudut Ru—C—O axial adalah bengkok sedikit. Nilai purata sudut Ru—C—O adalah 177.1° khatulistiwa dan nilai purata sudut Ru—C—O axial adalah 173.4°.

STRUCTURAL DETERMINATION AND ANALYSIS OF SOME NEW SCHIFF BASE AND *TRIANGULO*-TRIRUTHENIUM COMPOUNDS

ABSTRACT

Eight Schiff base compounds were studied in this research. They crystallized out in the common space groups, i.e. four compounds are in monoclinic *C*2/*c*, and one each in monoclinic *Cc*, $P2_1$ and *Pn* and triclinic $P\bar{1}$. One Schiff base compound exists in a zwitterion form. The structures of two Schiff base compounds are disordered. One Schiff base compound is a racemic twin crystal. Water solvent exists in the asymmetric unit of two Schiff base compounds. The Schiff base compounds all exist in an *E* configuration with respect to the N=C. The average N=C double bond value is 1.282 Å. Eighteen *triangulo*-triruthenium complexes were studied in this research. All of them crystallized out in the common space groups, i.e. seven compounds are in triclinic $P\bar{1}$, seven in monoclinic $P2_1/c$, two in monoclinic *C*2/*c*, and one each in orthorhombic *Pbca* and $Pca2_1$. The *triangulo*-triruthenium complex structures in four compounds are disordered. The asymmetric unit of eight compounds contains solvent molecules, e.g. water, dichloromethane or chloroform. All solvent molecules are disordered except for one of them. One *triangulo*-triruthenium compound is a racemic twin crystal and one *triangulo*-triruthenium compound is a pseudomerohedral twin crystal. In all *triangulo*-triruthenium complexes, the group 15 ligands occupy the equatorial position due to steric reaction. The effect of substitution results in significant differences in Ru—Ru bond lengths and carbonyl-ligands bond lengths and angles. The average three Ru—Ru bond lengths are 2.840 Å, 2.860 Å and 2.878 Å. The axial Ru—C bonds are longer than the equatorial Ru—C bonds. The average axial Ru—C bond lengths is 1.931 Å and the average equatorial Ru—C bond lengths is 1.892 Å. The bond length of equatorial

Ru—C when connected to the same Ru atom with the monodantate ligand is the shortest bond in most of the molecules. The average of these Ru—C bonds is 1.882 Å. The equatorial Ru—C—O angles are close to linear whereas the axial Ru—C—O angles are slightly bent. The average equatorial Ru—C—O angles is 177.1° and the axial Ru—C—O angles is 173.4°.

CHAPTER 1

INTRODUCTION

X-ray crystallography is a method of using a beam of X-ray to strike onto a crystal to determine the arrangement and geometrical parameters of atoms within a crystal (Fig. 1.1). The X-ray beams will be diffracted into many specific directions, and then with the angles and intensities of these diffracted beams, a crystallographer can produce a three-dimensional picture of the electron density within the crystal. From this electron density, the mean positions of the atoms in the crystal can be determined, as well as various information including connectivity, conformation, and bond lengths and angles. In addition, it gives information of the stoichiometry, the density, the symmetry and the three dimensional packing of the atoms in the solid.

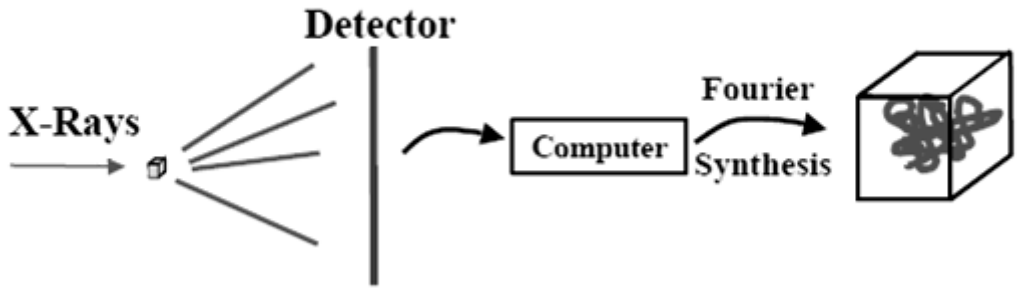

Fig. 1.1 The process of X-ray crystallography (Soman, 2007).

1.1 X-rays

X-ray is electromagnetic radiation with wavelength, λ, in the range of 0.1 to 100 Å (1 Å = 10^{-10} meters). X-rays have wavelengths similar to the dimensions of atoms (~1 Å) and therefore able to explore within crystals. X-rays are produced when fast-moving electrons collide with a metal target. The electron obtained enough energy to knock out an electron from the inner shell of the metal atom and as a result electrons from higher energy levels then fill up the vacancy and X-ray photons are emitted.

From $E = h\upsilon$

and $c = \upsilon\lambda$

$E = hc/\lambda$

where E is the energy, h is the Planck's constant, υ is the frequency of the X-ray, c is the velocity of light and λ is the wavelength.

Since X-rays have a very small wavelength, their energy is high enough for them to penetrate matter, the depth of penetrate depending on the density of the matter.

X-rays can be produced by a device called an X-ray tube (Fig. 1.2), cathode. There are two electrodes in an X-ray tube, an anode which is the metal target and a cathode with a tungsten filament which are situated in an evacuated chamber. Electrical current is passed through the tungsten filament and heating it to emit electrons. The electrons are accelerated to the anode target by high voltage applies across the electrodes. When the electrons strike the atoms in the target, the electron from the inner shell of the metal atom being knocked out and as a result

electrons from outer shell or higher energy levels then replace the vacancy and photons are emitted. This electronic transition results in the generation of X-rays. The X-rays then move through a beryllium window in the X-ray tube.

When the target material of the X-ray tube is bombarded with electrons accelerated from the cathode filament, two types of X-ray spectra are produced, the continuous and characteristic spectra. The characteristic spectra have been explained. The continuous spectra consist of a range of wavelengths of X-ray with minimum wavelength and intensity dependent on the target material and the voltage across the X-ray tube. The minimum wavelength decreases and the intensity increases as voltage increases.

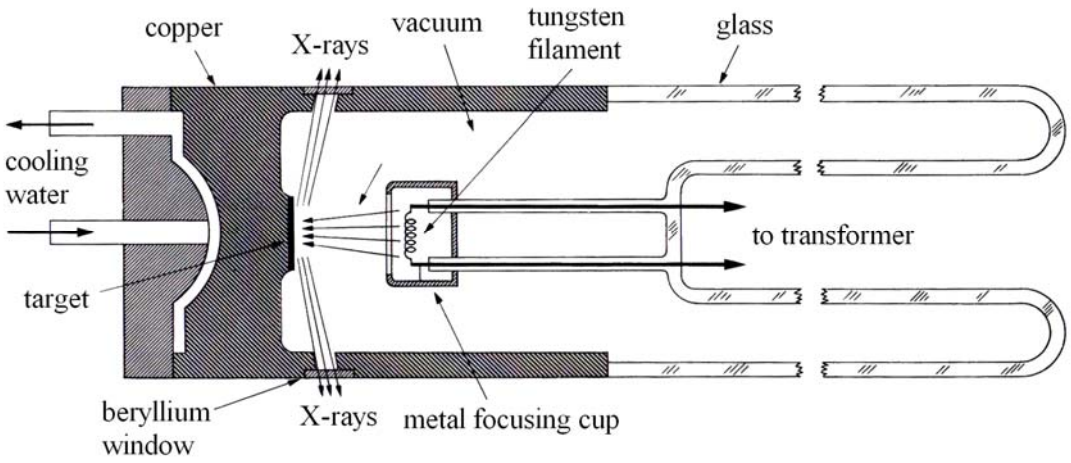

Fig. 1.2 Cross section of filament X-ray tube (Cullity, 1967).

1.2 Crystal Structure

A crystal structure is a solid substance consisting of an orderly arrangement of atoms repeated in the three-dimensional and bounded by plane faces. The structure of a crystal is described by space lattice and a basis with the basis of atoms assigned to each lattice point. The unit cell is the repeating volume of the lattice used to describe the crystal structure. It is characterized by six parameters, three axial lengths (a, b, c,) and three inter-axial angles (α, β, γ). The angle α is between b and c, β is between a and c, while γ is between a and b.

Crystals can be group into seven systems by the unit cell parameters which are triclinic, monoclinic, orthorhombic, tetragonal, trigonal, hexagonal and cubic. The crystal lattices are subdivided into 14 Bravais lattices and the basis can be assigned to 32 point groups. Combining the 14 Bravais lattices with the 32 point groups lead to 230 unique arrangements of motifs in space or 230 space groups.

1.3 Reciprocal Lattice

The X-ray diffraction patterns are interpreted in the form of reciprocal lattice. The relationship between the crystal lattice and the reciprocal lattice can be expressed in term of vectors (Glusker & Trueblood, 1985).

$$\boldsymbol{a}^* \cdot \boldsymbol{a} = 1; \boldsymbol{a}^* \cdot \boldsymbol{b} = \boldsymbol{a}^* \cdot \boldsymbol{c} = 0$$

$$\boldsymbol{a}^* = \frac{\boldsymbol{b} \times \boldsymbol{c}}{\boldsymbol{a} \cdot \boldsymbol{b} \times \boldsymbol{c}} = \frac{\boldsymbol{b} \times \boldsymbol{c}}{V} \qquad \boldsymbol{a} = \frac{\boldsymbol{b}^* \times \boldsymbol{c}^*}{\boldsymbol{a} \cdot \boldsymbol{b} \times \boldsymbol{c}} = \frac{\boldsymbol{b}^* \times \boldsymbol{c}^*}{V^*}$$

$$\boldsymbol{b}^* = \frac{\boldsymbol{c} \times \boldsymbol{a}}{\boldsymbol{a} \cdot \boldsymbol{b} \times \boldsymbol{c}} = \frac{\boldsymbol{c} \times \boldsymbol{a}}{V} \qquad \boldsymbol{b} = \frac{\boldsymbol{c}^* \times \boldsymbol{a}^*}{\boldsymbol{a} \cdot \boldsymbol{b} \times \boldsymbol{c}} = \frac{\boldsymbol{c}^* \times \boldsymbol{a}^*}{V^*}$$

$$\boldsymbol{c}^* = \frac{\boldsymbol{a} \times \boldsymbol{b}}{\boldsymbol{a} \cdot \boldsymbol{b} \times \boldsymbol{c}} = \frac{\boldsymbol{a} \times \boldsymbol{b}}{V} \qquad \boldsymbol{c} = \frac{\boldsymbol{a}^* \times \boldsymbol{b}^*}{\boldsymbol{a} \cdot \boldsymbol{b} \times \boldsymbol{c}} = \frac{\boldsymbol{a}^* \times \boldsymbol{b}^*}{V^*}$$

where $\boldsymbol{a}$, $\boldsymbol{b}$, $\boldsymbol{c}$ is the vector unit in crystal lattice, $\boldsymbol{a}^*$, $\boldsymbol{b}^*$, $\boldsymbol{c}^*$ is the vector unit in reciprocal lattice, V is the volume in crystal lattice and V^* is the volume of reciprocal lattice.

1.4 X-ray Diffraction

The diffraction of X-ray can be described by a simple equation which introduced by W. L. Bragg called Bragg's law (Fig. 1.3).

$$2d \sin \theta = n\lambda, \qquad n = 1, 2, 3, \ldots$$

where d is the lattice spacing, θ is the angle between the wavevector of the incident plane wave and the lattice planes, λ is its wave length and n is an integer, the order of the reflection.

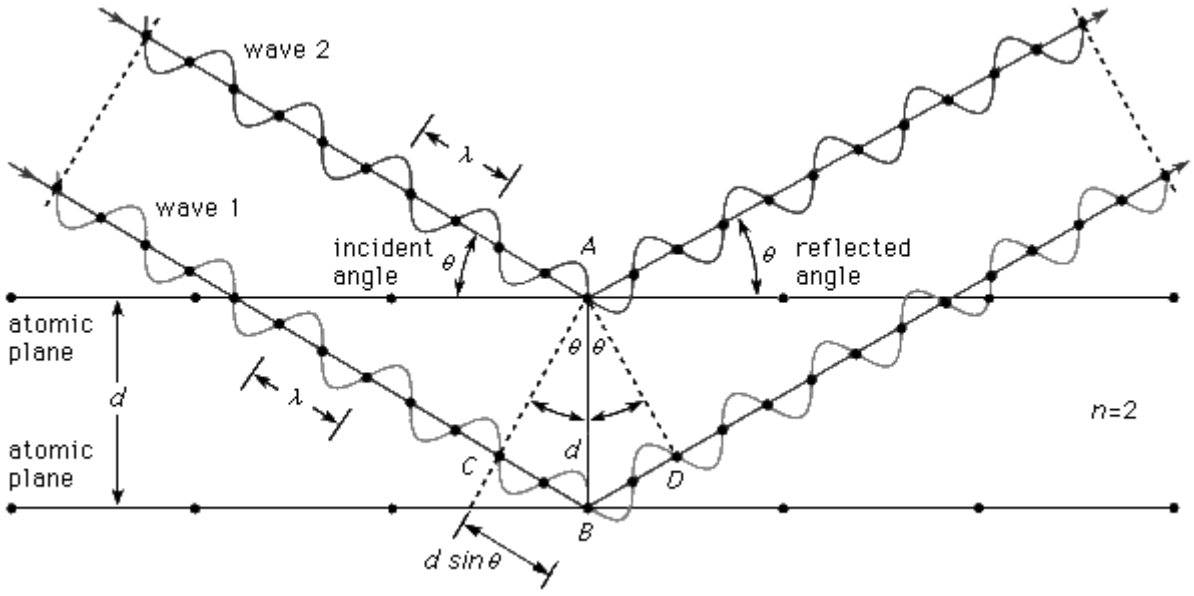

Fig. 1.3 Bragg's law diffraction (Bragg reflection, 2010).

Fig. 1.4 shows the Ewald sphere and the limiting sphere. The Ewald sphere construction shares the properties of Bragg's law. For a crystal and an X-ray beam of wavelength, λ, let $\mathbf{s}_o$ be the unit vector in the direction of the primary beam and **s** be the unit vector of the diffracted beam concerning a lattice plane with the normal vector **H**. The vectors **H**, $\mathbf{s}_o$ and **s** are related by the equation

$$\mathbf{H} = \frac{\boldsymbol{s} - \boldsymbol{s}_o}{\lambda}$$

It can be seen that

$$\frac{|\mathbf{H}|/2}{1/\lambda} = \sin\theta$$

with d = 1/|**H**|, we get $\lambda = 2d \sin\theta$ which is Bragg's law. For a diffraction to take place, Ewald states that a lattice plane L is in the diffraction position if its normal vector **H** lies on the surface of the Ewald sphere of radius $1/\lambda$ with the crystal at its center. For any reciprocal space vector, only those that fall on the surface of the Ewald sphere obey Bragg's law and therefore lead to diffraction.

Since the diameter of Ewald sphere is $1/\lambda$ only those reflections in reciprocal lattice space inside the sphere of radius $2/\lambda$ (the limiting sphere) can be observed. The radius of the limiting sphere is twice of that of the Ewald sphere (Fig. 1.4).

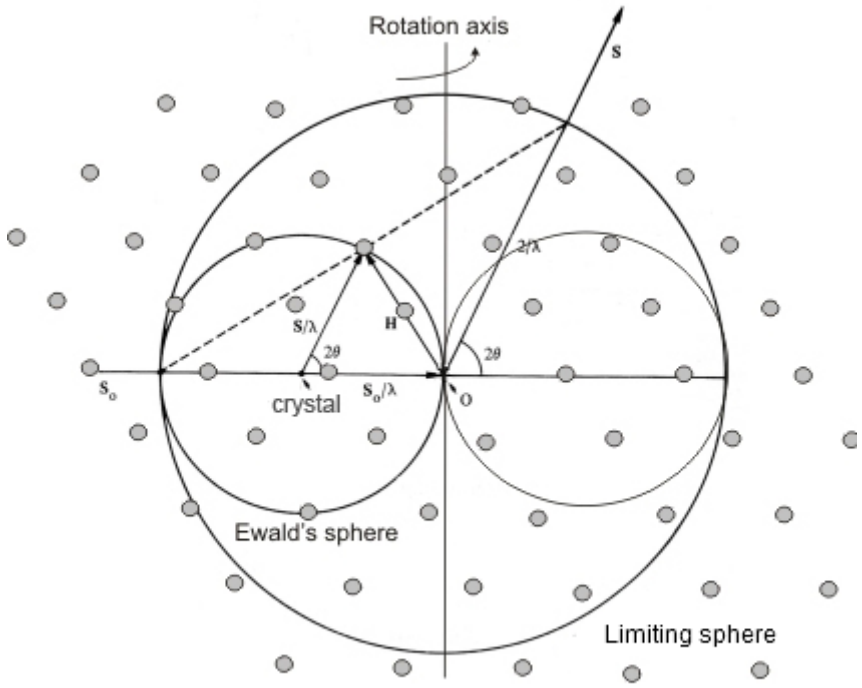

Fig 1.4 Ewald sphere, radius $1/\lambda$ and limiting sphere, radius $2/\lambda$ (Crystallography, 2009).

1.5 Superposition of waves

Each of the electrons in the crystal structure scatters a small fraction of the incident energy when a crystal is subjected to the electromagnetic field of an X-ray beam. By the principle of superposition, for these scattered waves combined to give the resultant wave reflected from each set of planes *hkl* (Stout & Jensen, 1989). It states that the amplitude resulting from the simultaneous action of several waves at a point is the sum of the displacements of the individual waves. The reflection of *hkl* consists of combined scattering waves by all atoms in the structure. An Argand diagram (Fig. 1.5) shows three waves with amplitudes f_1, f_2, f_3 and phase angles δ_1, δ_2, δ_3.

The x component of the resultant vector

$$x = f_1 \cos\delta_1 + f_2 \cos\delta_2 + f_3 \cos\delta_3 = \sum_{j=1}^{3} f_j \cos\delta_j \tag{1.1}$$

and correspondingly for the y component

$$y = f_1 \sin\delta_1 + f_2 \sin\delta_2 + f_3 \sin\delta_3 = \sum_{j=1}^{3} f_j \sin\delta_j \tag{1.2}$$

The magnitude of the resultant $|F|$ is

$$|F| = (x^2 + y^2)^{1/2} = \left[\left(\sum_{j=1}^{3} f_j \cos\delta_j \right)^2 + \left(\sum_{j=1}^{3} f_j \sin\delta_j \right)^2 \right]^{1/2} \tag{1.3}$$

and the phase angle is

$$\alpha = \tan^{-1} \frac{\sum_{j=1}^{3} f_j \sin\delta_j}{\sum_{j=1}^{3} f_j \cos\delta_j} \tag{1.4}$$

The result can be generalised to nth number of waves

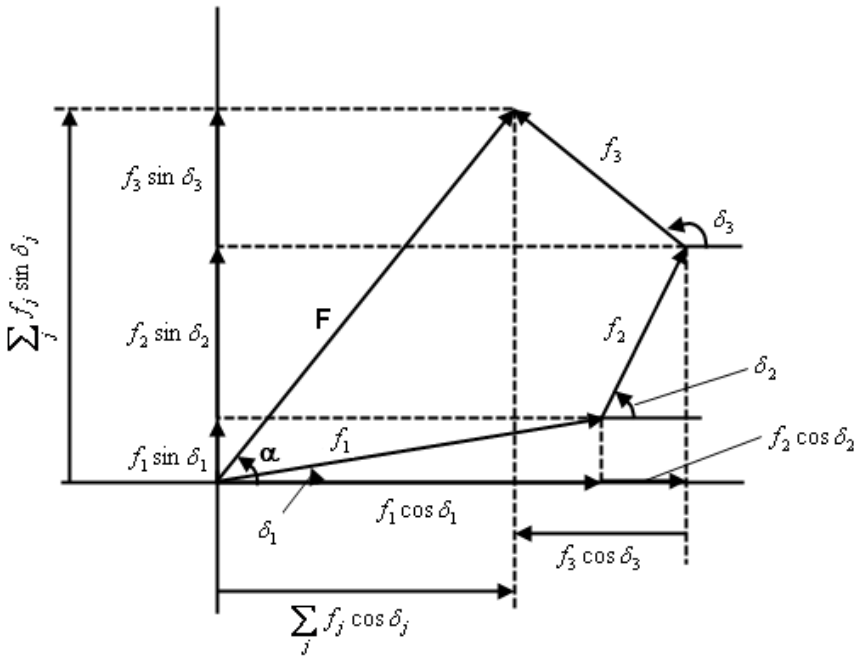

Fig. 1.5 Components on the coordinate axes of a sum of vectors are equal to the sums of the components of the individual vectors (Stout & Jensen, 1989).

1.6 Scattering Factor

The atomic scattering factor is needed to be considered in order to evaluate the combined scattering from the atoms in the unit cell. They are classified as functions of (sin θ)/λ and denoted as $f_{j,\theta}$ or just f_j. The atomic scattering factor depends upon the nature of the atom, the scattering direction, the wavelength of X-rays used and the thermal vibrations of the atom (Ladd & Palmer, 1979).

Figure 1.6 shows the general form of the atomic scattering factors. The atomic scattering factor, f, depends on the number of extranuclear electrons in the atom. The maximum value for a given atom j is Z_j, the atomic number of the jth atomic species. Along the direction of the incident beam (sin $\theta = 0$), f has maximum value is

$$f_{j,\theta(\theta=0)} = Z_j \tag{1.5}$$

f is measured in units of electrons.

Each atom in a structure vibrates due to thermal vibration of that particular atom in the structure. For simplicity, assuming isotropic vibration, the temperature factor correction to the atomic scattering factor for the jth atom is

$$T_{j,\theta} = \exp[-B_j(\sin^2\theta)/\lambda^2] \tag{1.6}$$

where B_j, the temperature factor of atom j, is given by

$$B_j = 8\pi^2\overline{U_j^2} \tag{1.7}$$

and $\overline{U_j^2}$ is the mean-square amplitude of vibration of the jth atom from its equilibrium position.

The temperature-corrected atomic scattering factor may be written as

$$g_j = f_{j,\theta} T_{j,\theta} \tag{1.8}$$

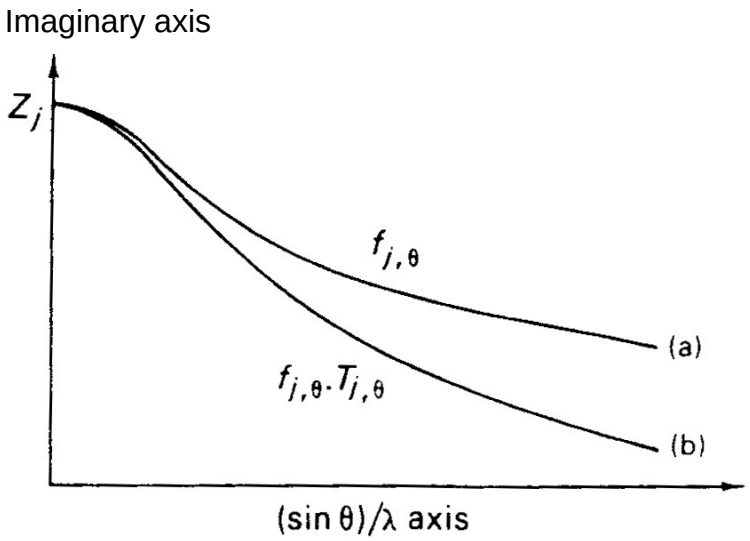

Fig. 1.6 Atomic scattering factors: (a) stationary atom, $f_{j,\theta}$ (b) atom corrected for thermal vibration, $f_{j,\theta} T_{j,\theta}$. (Ladd & Palmer, 1979).

1.7 Structure Factor

The structure factor, $\boldsymbol{F}_{hkl}$ is the resultant of N waves scattered in the direction of reflection hkl by the N atoms in the unit cell. Each of these waves have an amplitude proportional to the scattering factor of the atom, g_j and a phase, ϕ_j with respect to the origin of the unit cell (Stout & Jensen, 1989). Since the scattering factor of an atom is given in terms of an equivalent number of electrons, the structure factor is likewise measured in units of electrons. The total phase difference in radians between the origin and the point x, y, z is

$$\phi = 2\pi(hx + ky + lz)$$

Substitution in Eq. (1.3) gives for the magnitude of the structure factor

$$\left|F_{hkl}\right| = \left\{\left[\sum g_j \cos 2\pi(hx_j + ky_j + lz_j)\right]^2 + \left[\sum g_j \sin 2\pi(hx_j + ky_j + lz_j)\right]^2\right\}^{1/2} \tag{1.9}$$

$$\left|F_{hkl}\right| = (A_{hkl}^2 + B_{hkl}^2)^{1/2} \tag{1.10}$$

where

$$A_{hkl} = \sum g_j \cos 2\pi(hx_j + ky_j + lz_j) \tag{1.11}$$

and

$$B_{hkl} = \sum g_j \sin 2\pi(hx_j + ky_j + lz_j) \tag{1.12}$$

Compare with Eq. (1.4) and refering to Fig. (1.5) will show that A and B are the projections of $\boldsymbol{F}$ on the x and y axes of a Cartesian coordinate system, so we may write

$$\boldsymbol{F}_{hkl} = A_{hkl} + iB_{hkl} \tag{1.13}$$

Similarly, in view of Eq. (1.4), the phase of the resultant wave is

$$\alpha_{hkl} = \tan^{-1}\frac{B_{hkl}}{A_{hkl}} \tag{1.14}$$

The structure factor in exponential form is

$$\boldsymbol{F}_{hkl} = \sum_j g_j \exp(i\phi_j) = \sum_j g_j \exp[2\pi i(hx_j + ky_j + lz_j] \tag{1.15}$$

1.8 Friedel's Law

The centrosymmetric property of the diffraction pattern is stated by Friedel's law as $I(hkl) = I(\overline{hkl})$. The g_j will be the same for both hkl and $\overline{hkl}$ reflections because of it is a function of $[(\sin\theta)/\lambda]^2$, i.e.

$$g_{j,\theta} = g_{j,-\theta} \tag{1.16}$$

because reflection from opposite sides of any plane will occur at the same Bragg angle θ. From (1.15),

$$\boldsymbol{F}_{hkl} = \sum_j g_{j,\theta} \exp[2\pi i(hx_j + ky_j + lz_j] \tag{1.17}$$

and

$$\boldsymbol{F}_{\overline{hkl}} = \sum_j g_{j,-\theta} \exp[-2\pi i(hx_j + ky_j + lz_j] \tag{1.18}$$

From (1.13),

$$\boldsymbol{F}_{\overline{hkl}} = A_{\overline{hkl}} + iB_{\overline{hkl}} \tag{1.19}$$

where $A_{\overline{hkl}}$ and $B_{\overline{hkl}}$ are given by (1.11) and (1.12), respectively. It is known that $\cos(-\theta) = \cos\theta$ and $\sin(-\theta) = -\sin\theta$. Thus,

$$\boldsymbol{F}_{\overline{hkl}} = A_{\overline{hkl}} - iB_{\overline{hkl}} \tag{1.20}$$

Fig. 1.7 show the vectorial representations of $\boldsymbol{F}(hkl)$ and $\boldsymbol{F}(\overline{hkl})$ on an Argand diagram. Important relationships are:

$$\varphi(\overline{h}\overline{k}\overline{l}) = -\varphi(hkl) \tag{1.21}$$

$$|F(\mathrm{hkl})| = |F(\overline{hkl})| = [A'^2(hkl) + B'^2(hkl)]^{1/2} \tag{1.22}$$

Since $I(\mathrm{hkl}) \propto |F(\mathrm{hkl})|^2$, thus,

$$I(hkl) = I(\overline{hkl}) \tag{1.23}$$

which is Friedel's law.

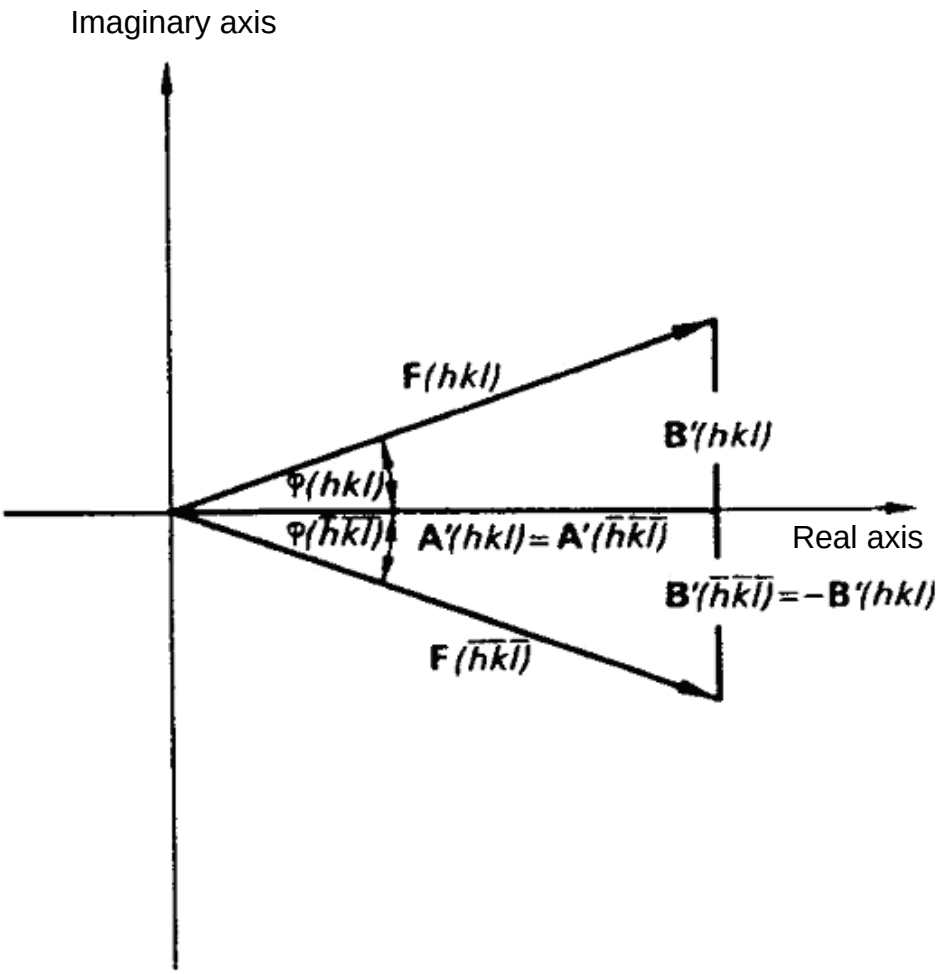

Fig. 1.7 Relationship between **F**(hkl) dan **F** ($\bar{h}\bar{k}\bar{l}$) leading to Friedel's law, from which $|F(\text{hkl})|=|F(\bar{h}\bar{k}\bar{l})|$ (Ladd & Palmer, 1979).

1.9 Electron Density

The electron density, ρ is the concentration of electrons in the vicinity of atoms in a crystal. It is often measured in electrons per $Å^3$. Atoms with high atomic numbers will have larger concentration of electrons compared to atoms of low atomic numbers (Ladd & Palmer, 1979).

Atoms appear as peaks in the electron density function and this peak position is assumed to correspond to its atomic centre. The heights of the peaks in an electron density distribution of a crystal are proportional to the corresponding atomic numbers. Situated at the extreme low end of the atomic numbers, the hydrogen atom does not appear in electron density representations. Its small electron density merges into the background density. Nevertheless, hydrogen atoms can be detected through the difference-Fourier technique. In general, the more complete and accurate the experimental $|F|$ data, the better will be the atomic resolution and the more precise the final structure model (Ladd & Palmer, 1979).

The general electron density function is expressed as a three-dimensional Fourier series, that is

$$\rho(x,y,z) = \frac{1}{V}\sum_h\sum_k\sum_l \boldsymbol{F}_{hkl} \exp[-2\pi i(hx_j + ky_j + lz_j)] \qquad (1.24)$$

where V is the unit-cell volume.

An alternative expression for a three-dimensional Fourier series can be obtained by noting that the structure factor can be written in the form

$$\boldsymbol{F}_{hkl} = \left|F_{hkl}\right| \exp(2\pi i \phi_{hkl}) \tag{1.25}$$

where ϕ_{hkl} is the phase angle in cycles. Substitution into Eq. (1.24) gives

$$\rho(x,y,z) = \frac{1}{V}\sum_h \sum_k \sum_l |\, F_{hkl}\,| \exp(2\pi i \phi_{hkl}) \exp[-2\pi i(hx+ky+lz)] \tag{1.26}$$

$$\rho(x,y,z) = \frac{1}{V}\sum_h \sum_k \sum_l |\, F_{hkl}\,| \exp[-2\pi i(hx+ky+lz) - \phi_{hkl}] \tag{1.27}$$

Expanding Eq. (1.27) in terms of sine and cosine, and then assuming that Friedel's law holds so that the sine terms cancel for pairs of $\boldsymbol{F}_{hkl}$ and $\boldsymbol{F}_{\overline{hkl}}$ leads to

$$\rho(x,y,z) = \frac{1}{V}\sum_h \sum_k \sum_l |\, F_{hkl}\,| \cos[2\pi(hx+ky+lz) - \phi_{hkl}] \tag{1.28}$$

To get the $\rho(x,y,z)$, both $|F_{hkl}|$ and ϕ_{hkl} are needed. The $|F_{hkl}|$ can be obtained from the intensity data from the experiment, but the corresponding phase ϕ_{hkl} is not directly measurable. Basically, there are two methods to obtain the phase ϕ_{hkl}:

(1) Patterson Method (Heavy atom method)

(2) Direct method

1.10 Patterson Method (Heavy Atom)

The very first solution to the phase problem was introduced by Arthur Lindo Patterson in 1934. He reported a new Fourier series which could be calculated directly from the experimental intensity data by introduced a new function $P(u, v, w)$ which defines a new space (the Patterson space) and derived a formula known as the Patterson function (a simplification of the information contained in the electron density function).

$$P(u,v,w) = \frac{1}{V}\sum_{h}\sum_{k}\sum_{l} | F_{hkl} |^2 \cos 2\pi(hu + kv + lw) \qquad (1.29)$$

The Patterson function removes the term containing the phases, and the amplitudes of the structure factors are replaced by their squares. It is thus a function that can be calculated immediately from the available experimental data. The Patterson function provides a map of interatomic vectors (relative atomic positions), the height of its maxima being proportional to the number of electrons of the atoms implied. A peak at the point *uvw* in a Patterson map indicates that atoms exist in the crystal at x_1, y_1, z_1 and x_2, y_2, z_2 such that $u = x_1 - x_2$, $v = y_1 - y_2$ and $w = z_1 - z_2$. The heights of the peaks are approximately proportional to the values of Z_iZ_j, in which Z_i is the atomic number of the atom at one end of the vector and Z_j that of the atom at the other end.

This feature means an advantage in detecting the positions of "heavy" atoms (with many electrons) in structures where the remaining atoms have lower atomic numbers. If a structure contains one or a few atoms of higher atomic number, these atoms will dominate the scattering process. These atoms can usually be located from the Patterson map and the phases of the entire structure will seldom be far from the phases of the heavy atom(s). The remainder of the structure will usually be

revealed in the resulting electron density map, leading to improved phases and better approximations to the structure.

Once the Patterson map is calculated, it has to be correctly interpreted (at least partially) to get the absolute positions (x, y, z) of the heavy atoms within the unit cell. These atomic positions can now be used to obtain the phases ϕ_{hkl} of the diffracted beams by inverting Eq. (1.28) and therefore this will allow the calculation of the electron density function $\rho(x, y, z)$.

The Patterson functions are restricted to certain rules (Stout & Jensen, 1989):-

1. All Patterson functions are centrosymmetric.
2. Their lattice type (P, C, F, etc.) is the lattice type of the original space group.
3. Their space group is derived from the original space group by replacing all translational symmetry elements (screw, glides) by the corresponding non-translational elements (axes, mirrors) and by adding a center of symmetry if it is not already present.

Although the majority of structural problems are now solved by direct methods, these methods sometimes fail. In addition, there exist problems, especially with macromolecules, that are too large for current direct methods. The alternative approaches generally involve analyzing the intensity data by way of the Patterson function.

1.11 Direct Methods

Direct phasing is now the most common and important method to solve structures. The result of 80-90% of the reported small-molecule structures are solved using direct methods.

A very important step in the development of direct methods was the formulation by Sayre of a relationship based only on these two assumptions (Massa, 2004): that the electron density in a structure can never have a negative value, and that it is concentrated in well defined maxima

$$F_{hkl} = \phi_{hkl} \sum\sum\sum F_{h'k'l'} \cdot F_{h-h',k-k',l-l'} \qquad (1.30)$$

This equation states that the structure factor for any reflection *hkl* can be calculated as the sum of the products of the structure factors of all pairs of reflections whose indices sum to it.

Karl and Hauptman develop the principle into a practical method which is used today more than any other method. For centrosymmetric structures, in which the phase problem is reduced to a "sign problem", for a so-called Σ_2 triplet of strong reflections contributing to the Sayre equation

$$S_{hkl} \approx S_{h'k'l'} \cdot S_{h-h',k-k',l-l'} \qquad (1.31)$$

where *S* is refer to sign. If both $S_{h'k'l'}$ and $S_{h-h',k-k',l-l'}$ have the same sign (positive or negative) it is probable that the sign of S_{hkl} is positive. When three strong reflections have a triplet relationship to one another, *hkl, h'k'l' and h-h',k-k',l-l'*, then the electron density must be concentrated at intervals of *d* for all three sets of lattice planes. If the phases of two of the reflections are known, then the phase of the third reflection is determined by them. Each Σ_2-relationship in fact gives the probability

that the sign of a reflection *hkl* is determined by those of *h'k'l' and h-h',k-k',l-l'*, the probability depending on how strong the three reflections are. For *N* atoms of equal weight in the unit cell, the probability *p*, that a phase is correctly determined is given by the relationship

$$P = 1/2 + 1/2 \tanh \left\{ 1/\sqrt{N} \left| E_{hkl} E_{h'k'l'} E_{h-h',k-k',l-l'} \right| \right\} \qquad (1.32)$$

where *E* is normalized structure factor. It is thus clear that direct methods work less well in principle for more complex structures. The limits for the method currently lie in the region of 200-300 non-hydrogen atoms in the asymmetric unit.

For noncentrosymmetric structures where there is no center of symmetry in a structure, then instead of a sign, a phase angle ϕ_{hkl} must be determined. In the general form of the Sayre equation, the structure factors are complex quantities, and an analogous to the sign relationship, a phase relationship may be derive

$$\phi_{hkl} \approx \phi_{h'k'l'} + \phi_{h-h',k-k',l-l'} \qquad (1.33)$$

The objective is to derive a phase ϕ_{hkl}, normally from a large number of Σ_2-relationship. Karle and Hauptman derived for this purpose the so-called tangent formula

$$\tan \phi_{hkl} = \frac{\sum_{h'k'l'} 1/\sqrt{N} \left| E_{hkl} E_{h'k'l'} E_{h-h',k-k',l-l'} \right| \cdot \sin(\phi_{h'k'l'} + \phi_{h-h',k-k',l-l'})}{\sum_{h'k'l'} 1/\sqrt{N} \left| E_{hkl} E_{h'k'l'} E_{h-h',k-k',l-l'} \right| \cdot \cos(\phi_{h'k'l'} + \phi_{h-h',k-k',l-l'})} \qquad (1.34)$$

(Massa, 2004)

1.12 Data Reduction

The collected data intensities consist of raw data from which crystal structures are derived. It represents all the information obtained from physical measurement on the crystal and further development of a structure depends on the skilful extraction of the information contained within the intensities. These raw intensities are corrected for various effects, a process referred to as data reduction (Stout & Jensen, 1989).

The amplitude of structure factor, $|F_{hkl}|$ is the most important quantity derived from the intensities. It is related to the experimentally observed intensities

$$\left|F_{hkl}\right| \propto \sqrt{I} \tag{1.35}$$

As we have described earlier, the structure factors are used to determine the positions of atoms from the electron density maps. It is customary to convert the intensities into "observed" structure amplitudes ($|F_o|=|F_{observed}|$) by a data reduction program and to use these as the observed data in subsequent calculations.

The relationship between $|F_{hkl}|$ and I depends on a number of factors. Normally, it is related to the individual reflection and the apparatus used to measure its intensity (Stout & Jensen, 1989). The proportionality of (1.35) can be rewritten as

$$\left|F_{hkl}\right| = (KI_{hkl} / Lp)^{1/2} \tag{1.36}$$

The term K depends on crystal size, beam intensity, and other fundamental constants. It is usually a constant for any given set of measurements and therefore omitted from data reduction.

The polarization factor, p is given by

$$p = \frac{(1+\cos^2 2\theta)}{2} \tag{1.37}$$

and is a simple function of 2θ, independent of the method of data collection except when a crystal monochromator is used. When a graphite monochromator is used, the reflection by the monochromator affects the direct beam before it reaches the crystal, and an additional factor Q must be introduced (Massa, 2004) to correct for the monochromator

$$p = \frac{(1+Q\cos^2 2\theta)}{(1+Q)} \tag{1.38}$$

The Lorentz factor, L is depends on the precise measurement technique used, given by

$$L = \frac{1}{\sin 2\theta} \tag{1.39}$$

Normally, these two effects are considered together as the so-called Lp-correction

$$Lp = \frac{(1+\cos^2 2\theta)}{(2\sin 2\theta)} \tag{1.40}$$

Thus, the observed structure factor $|F_o|$, on an arbitrary scale, may be calculated as

$$\left|F_o\right| = (I_{hkl} / Lp)^{1/2} \tag{1.41}$$

Corrections of absorption are potentially important. In an absorption process, the intensity, I of a beam after passing through a thickness t of absorber is given by

$$I = I_o e^{-\mu t} \tag{1.42}$$

where I_o is the intensity of the incident beam and μ is the linear absorption coefficient. To some extent they have become less significant with diffractometer data on small molecules with molybdenum radiation. It is because the coefficient is depended on the empirical formula, size of the crystal, and X-ray source used. In general, absorption correction is applied to improve the accuracy of the results, especially for crystal with large μ value.

1.13 Refinement

The principle of least squares states that the best value for the parameters are those that minimize the sums of the squares of the properly weighted differences between the observed and the calculated values of the function for all the observational points. The functional form of the structure factor is transcendental and so must be approximated by a truncated Taylor series (Stout & Jensen, 1989). Thus the quantity to be minimized is given by

$$D = \sum_{hkl} w_{hkl} (|F_o| - |kF_c|)^2 \qquad (1.43)$$

where w is the weight to be assigned an observation. In order to obtain the best fit, it will be necessary to consider a scale factor and the positional and temperature parameters of the atoms as variables that can be adjusted to minimize D. This gives a set of n equations in n unknown called the normal equations. These equations are linear equation.

The very weak reflections in an X-ray diffraction data set have relatively large errors and those for which the background exceeds the peak will have negative net intensities. They are undefined and cannot be used when refining against $|F_o|$. It is customary to eliminate the very weak reflections by use of a threshold reflections with intensities less than some positive threshold value such as $2\sigma(I)$ are given zero weight. The use of any threshold, however, introduces a bias in the data and is indefensible in principle; it is much better to refine against $|F_o|^2$ so that all data can be included. The function is minimized.

$$D' = \sum_{hkl} w'_{hkl} (|F_o|^2 - |kF_c|^2)^2 \qquad (1.44)$$

The weighting functions, w, should be a measure of the reliability of the observation. It has the effect of adjusting the contribution of each observation to the normal equations in such way as to produce the most reliable results. An example would be that the weight is equal to the reciprocal of the square of the standard deviation of the observation (Cruickshank, 1965; Hong & Robertson, 1985).

A useful index often output by least squares refinement programs is the so-called goodness of fit,

$$GOF = \left[\frac{\sum w(|F_o| - |F_c|)^2}{n - m} \right]^{1/2} \tag{1.45}$$

Sometimes it also termed as the standard deviation of an observation of unit weight. It is a measure of the degree to which the found distribution of differences between $|F_o|$ and $|F_c|$ fits the distribution expected from the weights used in the refinement. If these weights are correct, which implies that the errors in the data are strictly random and correctly estimated and if the model properly represents the structure that gives rise to the data, the value of the *GOF* is 1.0.